RSC Advances

PAPER

View Article Online
View Journal | View Issue

Cite this: *RSC Adv.*, 2020, **10**, 24764

A dual emission metal–organic framework for rapid ratiometric fluorescence detection of CO_3^{2-} in seawater†

Yu Wei[a] and Yan Xia *[abcd]

A dual emission metal–organic framework (IRMOF-10-Eu) was prepared and used as a ratiometric fluorescent sensor for CO_3^{2-} detection. IRMOF-10-Eu had good stability and excellent luminescence in aqueous solution. IRMOF-10-Eu showed dual fluorescence emission from the ligand and Eu^{3+} with single excitation. Upon treatment with CO_3^{2-}, the fluorescence ratio (I_{624}/I_{358}) of the probe displayed significant change. The relative fluorescence intensity ratio (I_{624}/I_{358}) and CO_3^{2-} concentration had a linear relationship in 50–300 μM range with a low detection limit of 9.58 μM. And the luminescence probe of CO_3^{2-} showed a fast detection time. The possible mechanism was investigated. CO_3^{2-} changed the structure of IRMOF-10-Eu and interrupted the energy transfer process. Thus, the fluorescence emission intensity of the ligand was increased and Eu^{3+} was decreased with the addition of CO_3^{2-}. IRMOF-10-Eu was used to detect CO_3^{2-} in seawater, which showed good prospect in practical application. Subsequently, a highly selective and sensitive probe, IRMOF-10-Eu, may pave an efficient way for CO_3^{2-} detection in seawater.

Received 20th March 2020
Accepted 17th June 2020

DOI: 10.1039/d0ra02581j

rsc.li/rsc-advances

1. Introduction

With the development of modern industry and the combustion of fossil fuel, the content of CO_2 in the atmosphere has increased year by year.[1] Ocean acidification is affected by the increase of the concentration of carbon dioxide in the atmosphere.[2] Carbonate ions are abundant and ubiquitous in the ocean.[3] Carbonates are important in maintaining pH in seawater and serve as essential components of skeletons, shells, and other marine structures.[4] It is vital to detect CO_3^{2-} in the cycle of carbon in ocean and environmental monitoring.[5] Therefore, it is urgent to develop an analytical method for the detection and quantification of CO_3^{2-}.

A variety of analytical methods have been reported for the identification of carbonate including ion selective electrodes,[6] Fourier transform infrared spectroscopy,[7] continuous-flow methods,[8] acoustic methods,[9] and coulorimetric methods.[10] However, these techniques were time-consuming, cumbersome and naked-eye-invisible. Because of high sensitivity, quick response, low cost, and real-time monitoring, much more attention has been paid to develop fluorescent probes for sensing carbonate. The single emission may be interfered by probe and analyte concentration and the excitation intensity.[11,12] Ratiometric fluorescence which possesses dual fluorescence emission alleviates the problem. And ratiometric fluorescence was used to detect a variety of targets, such as Al^{3+},[13] PO_4^{3-},[14] and aromatic pollutants.[15] Until now, due to its relative strong alkaline and large hydration free energy, only a few sensors have been reported for the detection of CO_3^{2-}. Thus, there is an urgent need to design a fluorescent probe that can highly selective and sensitive detect CO_3^{2-}.

A class of multifunctional hybrid materials, metal–organic frameworks (MOFs), were formed by metal ions or clusters and organic ligands. MOFs have triggered enormous interest for their high permanent porosity coupled with structural tunability,[16,17] large surface areas,[18,19] and luminescence.[20–25] Several strategies have been developed to synthesize MOF-based ratiometric sensors.[26] The design strategies mainly includes introducing luminescence metal ions, dyes and carbon dots (CDs) into singular MOFs. MOF-based ratiometric sensors exhibit emission centers from one metal center with one organic center, bimetallic centers, or two organic emission centers. Lanthanide ions (Ln^{3+}) is a commonly used metal emission center. However, Ln^{3+} luminescence is weak result from the forbidden f–f transition.[27–29] In order to solve it, intramolecular energy transfer from the organic ligands to the Ln^{3+} (antenna effect) was proposed, which can enhance the luminescence intensity and quantum yields of Ln^{3+} efficiently.[30–33] A dual emission MOF, IRMOF-10-Eu, was

[a]*Research Center for Analytical Sciences, College of Chemistry, Nankai University, Tianjin 300071, China. E-mail: nkxiayan@nankai.edu.cn; Fax: +86-22-23503034; Tel: +86 13602063491*

[b]*Key Laboratory of Biosensing and Molecular Recognition, China*

[c]*State Key Laboratory of Medicinal Chemical Biology, China*

[d]*Collaborative Innovation Center of Chemical Science and Engineering (Tianjin), China*

† Electronic supplementary information (ESI) available. See DOI: 10.1039/d0ra02581j

synthesized by two step. The advantages of IRMOF-10-Eu include the porosity of MOFs and the luminescence property of Ln^{3+} which can enhance sensitivity and the luminescence properties.

In this work, a fluorescence sensor, IRMOF-10-Eu, was developed for selective ratiometric fluorescence detection of CO_3^{2-}. The dual luminescence emission was derived from the ligand and Eu^{3+}, which decreased the environmental influence. Because CO_3^{2-} have an effect on the electronic structure of ligand, the selectivity of IRMOF-10-Eu was high in detecting CO_3^{2-}. CO_3^{2-} changed the relative fluorescence intensity ratio (I_{624}/I_{358}). The possible mechanism was investigated. CO_3^{2-} changed the structure of IRMOF-10-Eu and interrupted the energy transfer process. Thus, IRMOF-10-Eu can be a potential sensor for efficient detection of CO_3^{2-}.

2. Materials and methods

2.1 Reagents and chemicals

Zinc nitrate hexahydrate ($Zn(NO_3)_2 \cdot 6H_2O$, 99%) and europium(III) chloride hexahydrate ($EuCl_3 \cdot 6H_2O$, 99.99%) were supplied by Aladdin Chemistry Co. (Shanghai, China). 4,4′-Biphenyldicarboxylic acid (BPDC, 98%) was supported by Energy Chemical (Shanghai, China). *N*,*N*-Dimethylformamide (DMF, AR grade) and ethanol (AR grade) were purchased from Tianjin Concord technology Co., Ltd. (Tianjin, China). Sodium carbonate anhydrous (Na_2CO_3, 99.9%) was supported by Macklin Biochemical Co., Ltd. (Shanghai, China). Sodium hydrogen carbonate ($NaHCO_3$, 99.5%) was purchased from Meryer Chemical Technology Co. Ltd. (Shanghai, China). Aqueous solution of Na^+, K^+, Ca^{2+} and Mg^{2+} were prepared from corresponding chloride salts. Aqueous solution of F^-, Cl^-, Br^-, NO_3^-, PO_4^{3-}, $SO_4^{2-}$and HCO_3^- were prepared from corresponding sodium salts. These chloride salts and sodium salts were analytical reagent grade and obtained from Guangfu Fine Chemical Research Institute (Tianjin, China). Ultrapure water (18.2 MΩ cm) used throughout all experiments was purchased from Tianjin Physical and Chemical Analysis Center.

2.2 Instruments

The fluorescence spectra were obtained on a Hitachi Model FL-4500 fluorescence spectrometer using a quartz cell with a 1 cm path length at room temperature. The UV-vis absorption spectrum was recorded by a UV-3600 visible spectrophotometer (Shimadzu, Japan) at room temperature. A Rigaku Smart Lab diffractometer (Rigaku, Japan) was utilized to record powder X-ray diffraction spectrometry (PXRD) patterns with a 2θ range from 2–30° and monochromated Cu Kα radiation ($\lambda = 1.5418$ Å). A JSM-7500F scanning electron microscope (SEM) (JEOL, Japan) was used to obtain the morphology of the materials. Thermogravimetric analyses (TGA) were performed by a TG 8121 analyzer at heating rate of 15 °C min^{-1} from room temperature to 700 °C (Rigaku, Japan). A MAGNA-IR 560 spectrometer (Nicolet, USA) was used to recorded Fourier-transform infrared (FT-IR) spectrum in the range 3000–400 cm^{-1} with KBr tablet method. The mass spectral was recorded by 6520 Q-TOF LC/MS (Agilent, USA). An ICS-1100 ion chromatograph (IC) was used to measure anions in seawater, which equipped with Dionex IonPac™ AS14 column (Thermo, USA). The measurement of Eu^{3+} and mental ions in sea water was carried out on a Spectro Blue inductively coupled plasma-optical emission spectroscopy (ICP-OES) (Spectro, Germany).

2.3 Synthesis of IRMOF-10 and IRMOF-10-Eu

IRMOF-10 was synthesized according to the reported procedure.[34] Typically, 1.38 mmol zinc nitrate hexahydrate ($Zn(NO_3)_2 \cdot 6H_2O$) and 4,4′-biphenyldicarboxylic acid (BPDC, 0.3 g, 1.2 mmol) were stirred for 15 min in 20 mL of *N*,*N*-dimethylformamide (DMF). Then, the homogenous solution was poured into a Teflon lined steel autoclave, which was placed in a pre-heated oven at 100 °C for 8 h oven to yield rectangular prismatic crystals. Afterwards, it was separated by centrifugation and washed with DMF three times. And the product was immersed in chloroform for 3 days, during which the activation solvent was isolated, freshly replenished three times every day. The solvent was removed and the precipitate was dried in oven for 12 h under vacuum at 343 K.

IRMOF-10-Eu was facilely prepared by the mixture of 0.05 g IRMOF-10 and 0.3663 g $EuCl_3 \cdot 6H_2O$ in 8 mL ethanol at 60 °C for 24 h. The resulting white powder was centrifuged and washed with ethanol. The solid was dried at 353 K under a vacuum for 12 h.

2.4 UV-vis absorption, fluorescence excitation, and emission spectra of IRMOF-10-Eu

The concentration of the free ligand and IRMOF-10-Eu was 0.05 mg mL^{-1} for the absorption and luminescent property. For the UV-vis absorption, the scanning wavelength was set at the range from 800 nm to 200 nm and the split was 2.0. And the test solution was placed in cuvette (1 cm × 1 cm). To study the luminescent property, the slit of the free ligand and IRMOF-10-Eu was set at 5.0 nm × 5.0 nm and the PMT voltage was set at 700 V. And the excitation wavelength was set at 278 nm.

2.5 Day-to-day fluorescence stability and pH-dependence luminescent studies

The effects of time and pH were studied at 25 °C. The day-to-day fluorescence stability of IRMOF-10-Eu was prepared by IRMOF-10-Eu introducing in aqueous solution. After soaking for a predetermined time, the fluorescence data was collected. To study the pH-dependence luminescent, IRMOF-10-Eu was immersed in the aqueous solution, and the pH was adjusted with NaOH and HCl to the range of 2–10. The fluorescence data was collected after treatment for 5 min.

2.6 Ratiometric detection of carbonate ions

Luminescence responses of IRMOF-10-Eu toward CO_3^{2-} were investigated in their suspensions at room temperature. 1 mM aqueous solution of Na_2CO_3 was diluted to the final concentration ranging from 0 to 500 μM. Then 0.2 mg IRMOF-10-Eu was added in 4 mL aqueous solution of CO_3^{2-} and mixed well. After incubation for 5 min, their fluorescence spectra were recorded. For selectivity experiments, equal weight IRMOF-10-

Eu was soaked in 4 mL aqueous solution of metal ions (M = Na^+, Mg^{2+}, K^+ or Ca^{2+}, 500 μM) or anions (A = F^-, Cl^-, Br^-, NO_3^-, PO_4^{3-}, SO_4^{2-}, or HCO_3^-, 500 μM). The emission spectra of the mixtures were recorded after treatment for 5 min. To study the anti-interference ability of IRMOF-10-Eu, equal weight IRMOF-10-Eu was soaked in 4 mL mixed aqueous solution of CO_3^{2-} and mental ions (M = Na^+, Mg^{2+}, K^+, or Ca^{2+}, 500 μM) or anions (A = F^-, Cl^-, Br^-, NO_3^-, PO_4^{3-}, SO_4^{2-}, or HCO_3^-, 500 μM). After treatment for 5 min, the emission spectra of the mixtures were recorded.

2.7 Determination of carbonate detection in seawater

The seawater was collected from Wenchanghai, Yellow Sea, Yinggehai, and Beibu Gulf (China). To remove impurities, the seawater was filtered with 0.45 μm membranes. The 0.05 mg mL^{-1} sensor solution was prepared by introducing the IRMOF-10-Eu (0.5 mg) powder into 10 mL of the prepared seawater samples. After 5 min of incubation, the fluorescence emission data were collected.

3. Results and discussion

3.1 Characterization of IRMOF-10-Eu

As is shown in Fig. 1A, the PXRD pattern of IRMOF-10 was well matched with the simulated one, which indicated IRMOF-10 was prepared successfully.[35] The as-synthesized IRMOF-10 showed the typical peak at $2\theta = 5.98°$, which can be ascribed to the presence of a nonporous phase as a result of structural degradation induced by water. IRMOF-10-Eu also showed the typical peak at $2\theta = 5.98°$. Good agreement between IRMOF-10-Eu and IRMOF-10 PXRD pattern indicated that the framework of IRMOF-10-Eu still kept original type. Because Eu^{3+} was doped into the lattice, the peak at 8.24° had almost disappeared.[36] It can be observed in Fig. 1B, the SEM image of the IRMOF-10 showed rectangular prismatic crystals which had large dimension in the range of 30–40 μm. After the doped of Eu^{3+}, IRMOF-10-Eu showed flower-like crystal (Fig. 1C). Elemental mapping of IRMOF-10-Eu showed that Eu^{3+} was distributed in framework, which demonstrated Eu^{3+} was successfully doped in IRMOF-10-Eu (Fig S1†). As is shown in Fig. 1D, the TGA of IRMOF-10-Eu showed good thermal stability which was similar to IRMOF-10. Two events of weight losses were exhibited in the TGA curves. The first step gradual weight loss of 12.2% between 57 °C and 304 °C corresponded to the loss of coordinated H_2O and DMF molecules. In the second step, due to decomposition of the framework and the release of the ligand composite, the weight of IRMOF-10 and IRMOF-10-Eu decrease suddenly. Weight loss of 46.7% occurred in the range of 304–497 °C for IRMOF-10-Eu. The final residues are composed of Eu_2O_3 and ZnO.[37] In the range of 304–601 °C, weight loss of 61.1% occurred for IRMOF-10. The final residues are composed of ZnO.

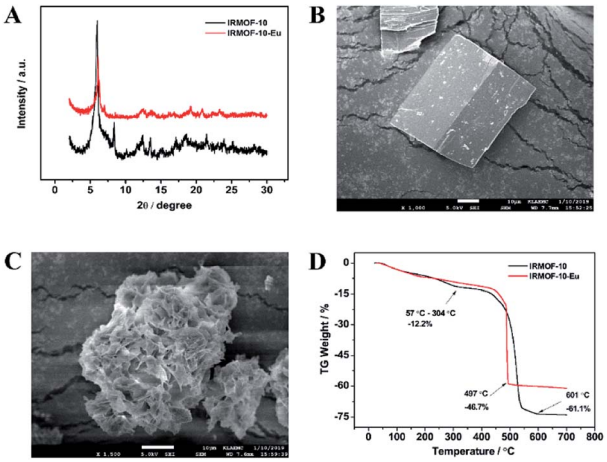

Fig. 1 (A) PXRD patterns of IRMOF-10 and IRMOF-10-Eu; SEM image of IRMOF-10 (B) and IRMOF-10-Eu (C); (D) TGA curve of IRMOF-10 and IRMOF-10-Eu.

3.2 Optical properties

The optical properties of IRMOF-10-Eu in aqueous solution were recorded at room temperature. As can be seen from Fig. S2,† due to the π–π* transition of BPDC, the excitation spectrum of the ligand and IRMOF-10-Eu showed absorption band centred at 250 nm and 278 nm, respectively. Thus, the excitation peak of IRMOF-10-Eu originated from BPDC. The spectrum of IRMOF-10-Eu displayed a slight red shift, which was derived from the extensive π-conjugated system formed between Zn^{2+} and BPDC.[38] The emission spectra of IRMOF-10-Eu was displayed in Fig. 2. IRMOF-10-Eu showed dual fluorescence emission from ligand and Eu^{3+} under excited at 278 nm. The emission spectra consist of emission of BPDC and the characteristic emission of Eu^{3+}. Eu^{3+} ions have remarkable spectroscopic properties. However, the emission intensity of free Eu^{3+} ions was weak with the direct excitation, because the ultraviolet light absorption was weakened by the f–f forbidden transition of Eu^{3+} ions. It is clearly shown in Fig. S3†, the emission property of BPDC and $EuCl_3$ was studied. A series of weak emission which appear at 599 nm ($^5D_0 \rightarrow {}^7F_1$), 624 nm ($^5D_0 \rightarrow {}^7F_2$) and 704 nm ($^5D_0 \rightarrow {}^7F_4$) were derived from Eu^{3+} upon excitation at 395 nm.[39] And BPDC showed strong luminescence intensity at 401 nm under excited at 250 nm. As

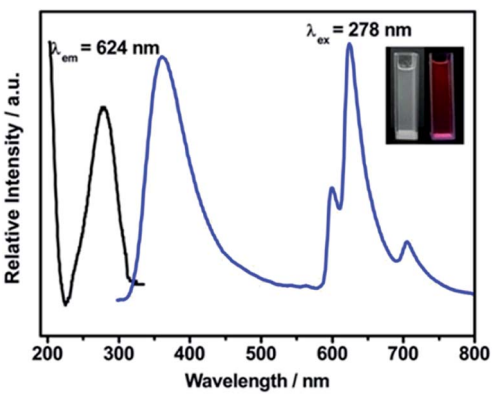

Fig. 2 The excitation and emission spectrum of IRMOF-10-Eu. Inset shows photograph of the mixture solution illustrate color under daylight (left) and ultraviolet light (right).

illustrated in Fig. S4†, under ultraviolet excitation, the electrons of ligand transit from S_0 state to S_1 state. Then intersystem crossing to T_1 state was occurred. Finally, the ligand T_1 state to Eu^{3+} ions was occurred in the process of energy transfer. Thus, emission from Eu^{3+} ions is observed. Above mentioned was antenna effect, which illustrate the strong emission of Eu^{3+} from IRMOF-10-Eu.[40] As illustrated in the inset photograph of Fig. 2, IRMOF-10-Eu dispersed in water was colorless under daylight. Under ultraviolet light, the mixture showed bright red luminescence. As is shown in Fig. S5†, the corresponding CIE chromaticity ($x = 0.54, y = 0.31$) of IRMOF-10-Eu was consistent with the color under ultraviolet light. The excitation spectra showed that IRMOF-10-Eu can absorb the ultraviolet light efficiently (Fig. 2).

The effect of pH on the fluorescence stability of IRMOF-10-Eu was investigated. In the pH range of 6–8, IRMOF-10-Eu showed good fluorescence stability in aqueous solution (Fig. S6†). As illustrated in Fig. 3, IRMOF-10-Eu had good day-to-day fluorescence stability within 2 weeks, indicating the good solvent stability of IRMOF-10-Eu in aqueous solution.

3.3 Ratiometric detection of carbonate ions

Carbonate ions was detected to investigate the potential application of IRMOF-10-Eu. Fig. S7† was the fluorescence spectra of the IRMOF-10-Eu in 100 μM CO_3^{2-} solution with different reaction time and the plot of the intensity ratio of I_{624}/I_{358} *versus* time. In the first 3 min, the fluorescence spectra of the mixed solution had a big change. After 3 min, it became stable. Thus, after 5 min of IRMOF-10-Eu interaction with CO_3^{2-}, the fluorescence spectra were recorded. Fig. 4A showed the emission spectra of IRMOF-10-Eu added in CO_3^{2-} solution with different concentration. The emission intensity at 358 nm enhanced progressively with the concentration of CO_3^{2-} increased (0–500 μM), but the emission at 624 nm was decreased. Energy transfer and structure of IRMOF-10-Eu can be influenced by CO_3^{2-}. The detailed explanation was discussed in the part of mechanism of carbonate detection. And the corresponding CIE chromaticity of IRMOF-10-Eu in the presence and absence of CO_3^{2-} was displayed in Fig. S8†, which showed the color change with the concentration of CO_3^{2-}

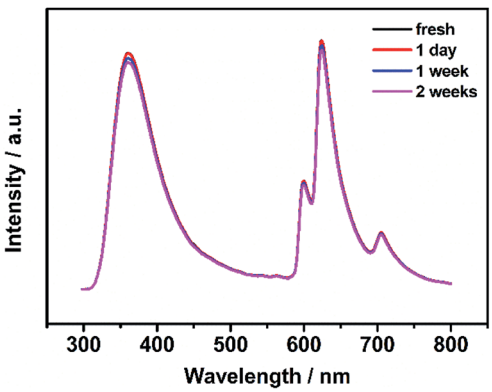

Fig. 3 Day-to-day fluorescence stability of IRMOF-10-Eu (0.05 mg mL^{-1}) under excitation at 278 nm.

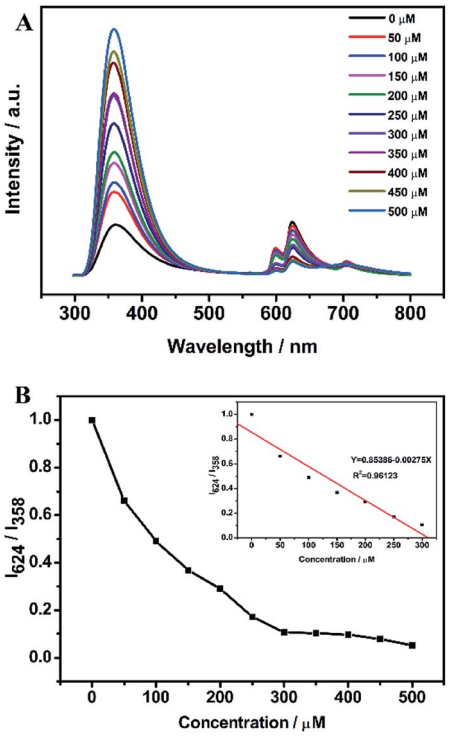

Fig. 4 (A) The emission spectra of IRMOF-10-Eu added in CO_3^{2-} solution with different concentration under excitation at 278 nm. (B) Plot of the relative luminescence intensity (I_{624}/I_{358}) *versus* the concentration of CO_3^{2-}.

increased. Fig. 4B showed the relationship between the intensity ratio of the emission at 624 and 358 nm (I_{624}/I_{358}) and CO_3^{2-} concentration in the range from 0 μM to 500 μM. In the range from 50 μM to 300 μM, a good linear correlation was obtained between I_{624}/I_{358} and CO_3^{2-} with a coefficient of $R^2 = 0.9612$. The calculation of detection limit was shown in Text S1.† The LOD was calculated to be 9.58 μM at a signal-to noise ratio of 3. As is shown in Table S1,† LOD was lower than the other methods, which shown that IRMOF-10-Eu had a great advantage in detecting CO_3^{2-}. Therefore, the dual-emission of IRMOF-10-Eu can quantitatively detect CO_3^{2-} through ratiometric fluorescence method.

It is important that the selectivity of IRMOF-10-Eu was investigated to evaluate the performance of the sensor. In regard to this, IRMOF-10-Eu was soaked in aqueous solutions of various common ions in seawater and recorded the fluorescence intensity. As is shown in Fig. 5, different degrees of changes on the luminescence intensity were observed while CO_3^{2-} caused the most significant change. According to the theory of Hard-Soft Acid-Base (HSAB theory),[41] the hard base (F^-) is prone to interact with the intermediate acid (Zn^{2+}) by Coulomb force, which resulted in the fluorescence change. After introducing different ions, the corresponding CIE chromaticity diagram was displayed in Fig. S9.† We can see that CO_3^{2-} caused significant emission color change. In addition, the absorption of IRMOF-10-Eu is increased with the addition of CO_3^{2-}, indicating the conformation change of BPDC induced by CO_3^{2-} (Fig S10A†). CO_3^{2-} decreased the efficiency of energy

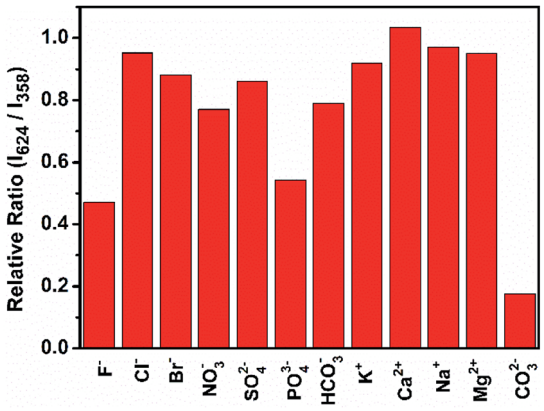

Fig. 5 Luminescence ratio of I_{624}/I_{358} from the responses of IRMOF-10-Eu in the presence of 300 μM carbonate ions and 500 μM interference ions.

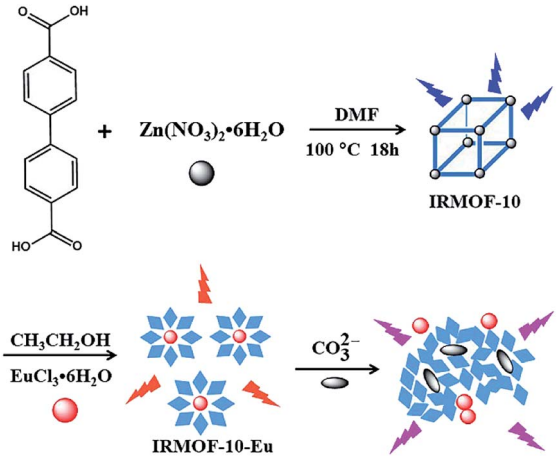

Scheme 1 A plausible mechanism for detection of CO_3^{2-} using IRMOF-10-Eu.

transfer between BPDC and Eu^{3+}. Thus, the emission of BPDC increased and Eu^{3+} decreased. In addition of other ions, the absorbance of IRMOF-10-Eu not obvious (Fig. S10B†). Due to the steric effect,[42] PO_4^{3-} which is large size triggered slight enhancement in absorbance. In summary, the selectivity of IRMOF-10-Eu was high in detecting CO_3^{2-}. To validate the anti-interference of IRMOF-10-Eu toward CO_3^{2-}, IRMOF-10-Eu was immersed in aqueous solution of different metal ions or anions with CO_3^{2-} ions. Fig. S11† showed that the foreign ions caused a negligible change compared with the pure CO_3^{2-} aqueous solutions. IRMOF-10-Eu can detect CO_3^{2-} well in the presence of foreign ions. Thus, IRMOF-10-Eu had a great potential for detecting CO_3^{2-}.

3.4 Mechanism of carbonate detection

To understand the carbonate detection mechanism of IRMOF-10-Eu, a series of experiments was explored. As can be seen in Table S2†, the concentration of Eu^{3+} in the aqueous solution was increased gradually as the concentration of CO_3^{2-} solution increased. It is assumed that CO_3^{2-} changed the structure of IRMOF-10-Eu, releasing free Eu^{3+}. Energy transfer process was disturbed and the transfer efficiency was decreased. The fluorescence intensity of Eu^{3+} was decreased (Scheme 1).

The phenomenon was proved by SEM. As shown in Fig. 1C, the morphology of IRMOF-10-Eu was flower-like crystal, which became slice after added CO_3^{2-} ions (Fig. S12†). The change suggested that CO_3^{2-} changed their structure.

XRD was explored to evidence the phenomenon also. Fig. S13† showed the XRD patterns of before and after immersed in CO_3^{2-} solution. After interacting with CO_3^{2-}, the typical peak 5.98° was shifted to 5.82°, which indicated the change of the crystal structure of IRMOF-10-Eu. Eu^{3+} released from IRMOF-10-Eu. Energy transfer process was disturbed. Thus, the emission of Eu^{3+} decreased.

Then, the UV-vis spectroscopic method was used to understand the fluorescence intensity at 358 nm which was increased as the concentration of CO_3^{2-} solution increased. As is shown in Fig. S14†, the absorption peak of BPDC at 241 nm. After the addition of CO_3^{2-}, the major absorption peak is increased and shifted to 278 nm. The red-shift and increasing absorption indicated that the conformation change of BPDC induced by CO_3^{2-}.[43] FT-IR was explored to study the phenomenon also. As can be seen from Fig. S15†, the peak of BPDC at 1508 cm^{-1} which was C=C stretching vibration in benzene ring[44] was disappear after the addition of CO_3^{2-}. It is evident that conjugation effect between BPDC and CO_3^{2-}. Then, we studied the absorption of IRMOF-10-Eu after the addition of CO_3^{2-}. As can be seen from Fig. S10A†, the absorption of IRMOF-10-Eu is increased with the addition of CO_3^{2-}. The phenomenon was proved by FT-IR. As is shown in Fig. S16†, the peak at 1607 cm^{-1}, 1577 cm^{-1}, 1525 cm^{-1} and 1405 cm^{-1} was C=C stretching vibration in benzene ring. After the addition of CO_3^{2-}, different degrees of changes on these peaks were observed. CO_3^{2-} had an effect on the C=C stretching vibration of the benzene ring. Because the metal–organic framework cannot be dissolved in organic solvents, we studied the mass spectrum of BPDC before and after the addition of CO_3^{2-} (Fig. S17†). The peak of BPDC does not change before and after interaction with CO_3^{2-}. It is evident that no host–guest complex form between CO_3^{2-} and BPDC. In summary, CO_3^{2-} influenced the conformation of aromatic ring in IRMOF-10-Eu and decreased the efficiency of energy transfer from ligand to Eu. And as the concentration of Eu^{3+} decreased, the energy transfer from BPDC to Eu^{3+} decreased.[45] Thus, the fluorescence intensity at 358 nm was increased gradually.

3.5 Detection of carbonate ions in real samples

The potential of IRMOF-10-Eu for CO_3^{2-} detection in sea water was evaluated. The sea water was chosen as real sample, which contained carbonate and other ions. ICP-OES and ion chromatography methods demonstrated that real sea water mainly contained Na^+, Ca^{2+}, K^+, Mg^{2+}, Sr^{2+}, Cl^-, Br^-, NO_3^-, PO_4^{3-}, SO_4^{2-}, which was listed in Table S3.† The most cation in seawater was sodium ions and the most anion was chloride ion. IRMOF-10-Eu was used to detect CO_3^{2-} in sea water. As can be

Table 1 Results of CO_3^{2-} detection in seawater ($n = 3$)

Sea area	Titrimetric analysis (μM)	This method (μM)
Yinggehai	294.5	286.7
Wenchanghai	233.2	258.4
Beibu Gulf	223.1	278.5
Yellow Sea	114.1	142.3

seen in Table 1, the results of ratiometric fluorescence method were corresponded with those from titrimetric analysis. Thus, IRMOF-10-Eu had a great potential to detect CO_3^{2-} in sea water.

To detect CO_3^{2-} conveniently and quickly, a test plate was prepared. IRMOF-10-Eu was dispersed in 0.5% aqueous carboxymethylcellulose sodium (CMC) and ultrasound for 5 min to form a uniform suspension, which was coated on the glass plate to form a film. Then the testing solvents were added to the test strip. After contact for 5 min, the content of CO_3^{2-} was judged rapidly by naked eyes with observable color change under the irradiation of UV light of 254 nm (Fig. S18†).

4. Conclusions

In summary, this work represents a ratiometric fluorescent sensor (IRMOF-10-Eu) for selective and quantitative detection of CO_3^{2-}. Characterization and optical properties of IRMOF-10-Eu was studied. IRMOF-10-Eu had good stability and excellent luminescence in aqueous solution. IRMOF-10-Eu displayed dual-emission under single excitation at 278 nm. After interacting with CO_3^{2-}, the emission of ligand was increased and Eu^{3+} was decreased. The relative fluorescence intensity ratio and CO_3^{2-} concentration have linear relationship with wide detection range and low detection limit. Because CO_3^{2-} have an effect on the electronic structure of BPDC, the selectivity of IRMOF-10-Eu was high in detecting CO_3^{2-}. The possible detection mechanism can be explained by energy transfer and structural change. IRMOF-10-Eu can be a promising sensor for the detection of CO_3^{2-} under real conditions in the future.

Conflicts of interest

The authors have declared no conflict of interest.

Acknowledgements

This work was supported by National Natural Science Foundation of China (21874073).

References

1 N. Tir, M. M. Al Ezzi, H. M. Abdullah, M. Yusupov, S. Kouser, H. Bahlouli and Z. H. Yamani, Detection of CO_2 using CNT-based sensors: role of Fe catalyst on sensitivity and selectivity, *Mater. Chem. Phys.*, 2017, **186**, 353–364.
2 R. A. Feely, S. R. Alin, J. Newton, C. L. Sabine, M. Warner, A. Devol, C. Krembs and C. Maloy, The combined effects of ocean acidification, mixing, and respiration on pH and carbonate saturation in an urbanized estuary, *Estuar. Coast Shelf Sci.*, 2010, **88**, 441–449.
3 V. Thimaradka, S. Pangannaya, M. Mohan and D. R. Trivedi, Hydrazinylpyridine based highly selective optical sensor for aqueous source of carbonate ions: electrochemical and DFT studies, *Spectrochim. Acta, Part A*, 2018, **193**, 330–337.
4 L. He, C. Liu and J. H. Xin, A novel turn-on colorimetric and fluorescent sensor for Fe^{3+} and Al^{3+} with solvent-dependent binding properties and its sequential response to carbonate, *Sens. Actuators, B*, 2015, **213**, 181–187.
5 A. Ghorai, J. Mondal, R. Chandra and G. K. Patra, A reversible fluorescent-colorimetric chemosensor based on a novel Schiff base for visual detection of CO_3^{2-} in aqueous solution, *RSC Adv.*, 2016, **6**, 72185–72192.
6 H. K. Lee, H. Oh, K. C. Nam and S. Jeon, Urea-functionalized calix[4]arenes as carriers for carbonate-selective electrodes, *Sens. Actuators, B*, 2005, **106**, 207–211.
7 W. Liu, Z. Sun, M. Ranheimer and H. Tang, A flexible method of carbonate determination using an automatic gas analyzer equipped with an FTIR photoacoustic measurement chamber, *Analyst*, 1999, **124**, 361–365.
8 M. Zougagh, A. Ríos and M. Valcárcel, Direct determination of total carbonate salts in soil samples by continuous-flow piezoelectric detection, *Talanta*, 2005, **65**, 29–35.
9 O. Dóka, D. Bicanic, M. Szücs and M. Lubbers, Direct measurement of carbonate content in soil samples by means of CO laser infrared photoacoustic spectroscopy, *Appl. Spectrosc.*, 1998, **52**, 1526–1529.
10 K. M. Johnson, A. Kortzinger, L. Mintrop, J. C. Duinker and D. W. R. Wallace, Coulometric total carbon dioxide analysis for marine studies: measurement and internal consistency of underway TCO_2 concentrations, *Mar. Chem.*, 1999, **67**, 291–303.
11 X. F. Yang, H. Qi, L. Wang, Z. Su and G. Wang, A ratiometric fluorescent probe for fluoride ion employing the excited-state intramolecular proton transfer, *Talanta*, 2009, **80**, 92–97.
12 F. Ye, C. Wu, Y. Jin, Y. H. Chan, X. Zhang and D. T. Chiu, Ratiometric temperature sensing with semiconducting polymer dots, *J. Am. Chem. Soc.*, 2011, **133**, 8146–8149.
13 J. N. Ha and B. Yan, Amino-decorated lanthanide(III) organic extended frameworks for multi-color luminescence and fluorescence sensing, *J. Mater. Chem. C*, 2014, **2**, 6758–6764.
14 X. Lian and B. Yan, A postsynthetically modified MOF hybrid as a ratiometric fluorescent sensor for anion recognition and detection, *Dalton Trans.*, 2016, **45**, 18668–18675.
15 X. Lian and B. Yan, A lanthanide metal–organic framework (MOF-76) for adsorbing dyes and fluorescence detecting aromatic pollutants, *RSC Adv.*, 2016, **6**, 11570–11576.
16 Y. Hijikata, S. Horike, M. Sugimoto, M. Inukai, T. Fukushima and S. Kitagawa, Pore design of two-dimensional coordination polymers toward selective adsorption, *Inorg. Chem.*, 2013, **52**, 3634–3642.

17 H. Li, J. Ren, X. F. Xu, L. M. Ning, R. Y. Tong, Y. Song, S. Y. Liao, W. Gu and X. Liu, A dual-responsive luminescent metal–organic framework as a recyclable luminescent probe for the highly effective detection of pyrophosphate and nitrofurantoin, *Analyst*, 2019, **144**, 4513–4519.

18 O. K. Farha, I. Eryazici, N. C. Jeong, B. G. Hauser, C. E. Wilmer, A. A. Sarjeant, R. Q. Snurr, S. T. Nguyen, A. O. Yazaydin and J. T. Hupp, Metal–organic framework materials with ultrahigh surface areas: Is the sky the limit?, *J. Am. Chem. Soc.*, 2012, **134**, 15016–15021.

19 H. K. Chae, D. Y. Siberio-Perez, J. Kim, Y. Go, M. Eddaoudi, A. J. Matzger, M. O'Keeffe and O. M. Yaghi, A route to high surface area, porosity and inclusion of large molecules in crystals, *Nature*, 2004, **427**, 523–527.

20 S. J. Qin, J. N. Hao, X. Y. Xu, X. Lian and B. Yan, Highly sensing probe for biological metabolite of benzene series pollutants based on recyclable Eu^{3+} functionalized metal–organic frameworks hybrids, *Sens. Actuators, B*, 2017, **253**, 852–859.

21 B. Wang, J. H. Liu, J. M. Yu, J. Lv, C. Dong and J. R. Li, Broad spectrum detection of veterinary drugs with a highly stable metal–organic framework, *J. Hazard. Mater.*, 2019, **382**, 121018–121026.

22 Q. J. Liu, H. Wang, P. Han and X. Y. Feng, Fluorescent aptasensing of chlorpyrifos based on the assembly of cationic conjugated polymer-aggregated gold nanoparticles and luminescent metal–organic frameworks, *Analyst*, 2019, **144**, 6025–6032.

23 X. Y. Xu and B. Yan, Eu(III) functionalized Zr-based metal–organic framework as excellent Fluorescent probe for Cd^{2+} detection in aqueous environment, *Sens. Actuators, B*, 2016, **222**, 347–353.

24 D. M. Chen, C. X. Sun, Y. Peng, N. N. Zhang, H. H. Si, C. S. Liu and M. Du, Ratiometric fluorescence sensing and colorimetric decoding methanol by a bimetallic lanthanide-organic framework, *Sens. Actuators, B*, 2018, **265**, 104–109.

25 L. V. Meyer, F. Schonfeld and K. Muller-Buschbaum, Lanthanide based tuning of luminescence in MOFs and dense frameworks – from mono- and multimetal systems to sensors and films, *Chem. Commun.*, 2014, **50**, 8093–8108.

26 S. Y. Wu, H. Min, W. Shi and P. Cheng, Multicenter metal–organic framework-based ratiometric fluorescent sensors, *Adv. Mater.*, 2019, **32**, 1805871.

27 M. D. Allendorf, C. A. Bauer, R. K. Bhakta and R. J. T. Houk, Luminescent metal–organic frameworks, *Chem. Soc. Rev.*, 2009, **38**, 1330–1352.

28 X. L. Zhang, Z. Y. Zhan, X. Y. Liang, C. Chen, X. L. Liu, Y. J. Jia and M. Hu, Lanthanide MOFs constructed from mixed dicarboxylate ligands as selective multi-responsive luminescent sensors, *Dalton Trans.*, 2018, **47**, 3272–3282.

29 M. Pan, Y. X. Zhu, K. Wu, L. Chen, Y. J. Hou, S. Y. Yin, H. P. Wang, Y. N. Fan and C. Y. Su, Epitaxial growth of hetero-Ln-MOF hierarchical single crystals for domain- and orientation-controlled multicolor luminescence 3D coding capability, *Angew. Chem., Int. Ed.*, 2017, **56**, 14582–14586.

30 L. Yi, L. N. Zhu, B. Ding, P. Cheng, D. Z. Liao, S. P. Yan and Z. H. Jiang, Six- and four-coordinated zinc(II) complexes exhibit strong blue fluorescent properties, *Inorg. Chem. Commun.*, 2003, **6**, 1209–1212.

31 S. G. Liu, J. L. Zuo, Y. Wang, Y. Z. Li and X. X. You, Synthesis, crystal structure and blue electroluminescence of a new zinc complex based on 2,6-bis(benzimidazolyl)pyridine, *J. Phys. Chem. Solids*, 2005, **66**, 735–740.

32 I. M. M. de Carvalho, E. D. Moreira and M. H. Gehlen, Synthesis, characterization, and photophysical studies of new bichromophoric ruthenium(II) complexes, *Inorg. Chem.*, 2003, **42**, 1525–1531.

33 M. Haga, T. Takasugi, A. Tomie, A. M. Ishizuya, T. Yamada, M. D. Hossain and M. Inoue, Molecular design of a proton-induced molecular switch based on rod-shaped Ru dinuclear complexes with bis-tridentate 2,6-bis(benzimidazol-2-yl) pyridine derivatives, *Dalton Trans.*, 2003, 2069–2079.

34 L. M. Eddaoudi, J. Kim, N. Rosi, D. Vodak, J. Wachter, M. O. Keeffe and O. M. Yaghi, Systematic design of pore size and functionality in isoreticular MOFs and their application in methane storage, *Science*, 2002, **295**, 469–472.

35 I. Gutierrez, E. Díaz and S. Ordonez, Consequences of cavity size and palladium addition on the selective hydrogen adsorption in isoreticular metal–organic frameworks, *Thermochim. Acta*, 2013, **567**, 79–84.

36 X. Y. Min, X. Wu, P. H. Shao, Z. Ren, L. Ding and X. B. Luo, Ultra-high capacity of lanthanum-doped UiO-66 for phosphate capture: unusual doping of lanthanum by the reduction of coordination number, *Chem. Eng. J.*, 2019, **358**, 321–330.

37 J. N. Hao and B. Yan, Amino-decorated lanthanide(III) organic extended frameworks for multi-color luminescence and fluorescence sensing, *J. Mater. Chem. C*, 2014, **2**, 6758–6764.

38 Z. R. Yang, M. M Wang, X. S. Wang and X. B. Yin, Boric-acid-functional lanthanide metal–organic frameworks for selective ratiometric fluorescence detection of fluoride ions, *Anal. Chem.*, 2017, **89**, 1930–1936.

39 X. T. Rao, Q. Huang, X. L. Yang, Y. J. Cui, Y. Yang, C. D. Wu, B. L. Chen and G. D. Qian, Color tunable and white light emitting Tb^{3+} and Eu^{3+} doped lanthanide metal–organic framework materials, *J. Mater. Chem.*, 2012, **22**, 3210–3214.

40 J. D. Einkauf, T. T. Kelley, B. C. Chan and D. T. de Lill, Rethinking sensitized luminescence in lanthanide coordination polymers and MOFs: band sensitization and water enhanced Eu luminescence in $[Ln(C_{15}H_9O_5)_3(H_2O)_3]_n$ (Ln = Eu, Tb), *Inorg. Chem.*, 2016, **55**, 7920–7927.

41 B. X. Xiao, Q. Q. Zhang, C. Z. Huang and Y. F. Li, Luminescent Zn(II)-terpyridine metal–organic gel for visual recognition of anions, *RSC Adv.*, 2015, **5**, 2857–2860.

42 X. L. Zeng, J. Hu, M. Zhang, F. L. Wang, L. Wu and X. D. Hou, Visual detection of fluoride anions using mixed lanthanide metal–organic frameworks with a smartphone, *Anal. Chem.*, 2020, **92**, 2097–2102.

43 A. A. Bahajaj and A. M. Asiri, Photochromic properties of (E)-3-(2-adamantylidene)-2-[5-(4-diethylaminophenyl)-2-methyl-

3-furylethylidene] succinic anhydride doped in polystyrene film, *Pigm. Resin Technol.*, 2008, **37**, 140–144.

44 M. M. Julie, T. Prabhu, S. S. Margreat, D. R. Leenaraj, S. Periandy, S. Muthu and B. R. Raajaraman, An antipsychotic drug: spectroscopic identification, structural features, DFT computations and molecular docking studies on 4-(methylamino)-3-nitrobenzoic acid, *J. Mol. Struct.*, 2019, **1196**, 33–41.

45 Y. H. Zhang, B. Li, H. P. Ma, L. M. Zhang, H. Jiang, H. Song, L. G. Zhang and Y. S. Luo, A nanoscaled lanthanide metal–organic framework as a colorimetric fluorescence sensor for dipicolinic acid based on modulating energy transfer, *J. Mater. Chem. C*, 2016, **4**, 7294–7301.